Journal of Materials Chemistry C

ROYAL SOCIETY OF CHEMISTRY

PAPER

View Article Online
View Journal | View Issue

Cite this: J. Mater. Chem. C, 2023, 11, 5987

Cationic tetraphenylethylene-based AIE-active acrylonitriles: investigating the regioisomeric effect, mechanochromism, and wash-free bioimaging†

Xiaoyuan Tian,[ab] Hui Wang,[d] Shixian Cao,[ab] Yunting Liu,[ab] Fanda Meng,*[c] Xiaoyan Zheng *[d] and Guangle Niu *[abd]

Developing regioisomeric organic fluorescent materials with tunable photophysical properties is particularly important in diverse applications. Here we synthesized three cationic regioisomeric aggregation-induced emission (AIE)-active acrylonitriles (*o*-TPE-ANPy$^+$, *m*-TPE-ANPy$^+$, and *p*-TPE-ANPy$^+$) by conjugation with tetraphenylethylene at different *ortho*/*meta*/*para* positions. The regioisomerism remarkably impacted their photophysical characteristics and solid-state intermolecular interactions. The regioisomeric AIE luminogens (AIEgens) exhibited faint emissions in solution but boosted fluorescence behaviors in the solid state. *o*-TPE-ANPy$^+$ and *m*-TPE-ANPy$^+$ showed similar yellow solid-state emissions with a fluorescence quantum yield (QY) of 14.3% and 1.8%, respectively. However, due to the strong intermolecular charge transfer effect, *p*-TPE-ANPy$^+$ exhibited a red-shifted solid-state emission of 616 nm (QY of 17.2%). In addition, *m*-TPE-ANPy$^+$ and *p*-TPE-ANPy$^+$ exhibited larger fluorescence enhancements toward viscosity than *o*-TPE-ANPy$^+$. Moreover, *o*-TPE-ANPy$^+$ was applied for achieving reversible mechanochromic performance with fluorescence changing from yellow to orange. Further use of these biocompatible AIEgens for wash-free and light-up imaging of mitochondria was successfully demonstrated. These interesting results facilitate a better understanding of the structure–property relationships in fluorescent regioisomers.

Received 10th December 2022,
Accepted 4th April 2023

DOI: 10.1039/d2tc05266k

rsc.li/materials-c

Introduction

Recent years have witnessed increasing developments and widespread applications of organic solid-state fluorescent materials in organic light-emitting diodes (OLEDs), memory devices, fluorescent sensors, and bioimaging.[1–8] Generally, conventional organic materials, such as coumarins, xanthenes, and so on, show significantly decreased fluorescence in the solid state, due to the aggregation-caused fluorescence quenching effect resulting from strong intermolecular π–π interactions.[9–11] To minimize the undesired fluorescence quenching effect, significant efforts have been devoted to constructing solid-state emissive materials, such as the introduction of large steric bulky groups in the structural skeleton and molecular dispersion in a host matrix.[12,13] However, some problems of complicated synthesis procedures and insufficient fluorescence brightness in the solid state were still encountered. Thus, developing anti-quenching fluorescent materials with inherent solid-state emissive advantage is in high demand.

The discovery of a unique photophysical phenomenon of aggregation-induced emission (AIE), the conception of which was proposed by Tang and co-workers in 2001,[14] provides new insights in this regard.[15–19] AIE luminogens (AIEgens) are non-fluorescent or faintly emissive in solution, yet they become highly emissive in the aggregate and solid states, due to the restriction of intramolecular motions (RIM).[17] Guided by the RIM mechanism, various structure-tunable AIEgens have been constructed to access different functionalities.[20–28] Among these, tetraphenylethylene (TPE) is a star AIEgen, and has been widely used and functionalized for diverse applications.[29–31] Increasing literature shows that regioisomerism has become a significant design concept, which significantly impacts the photophysical and chemical properties of fluorescent materials.[32–38] Indeed, some regioisomers based on TPE derivatives have been synthesized and investigated (Scheme 1).[39–46] For example,

[a] State Key Laboratory of Crystal Materials, Shandong University, Jinan 250100, P. R. China. E-mail: niugl@bit.edu.cn
[b] Suzhou Research Institute, Shandong University, Suzhou 215123, P. R. China
[c] School of Clinical and Basic Medical Sciences, Shandong First Medical University& Shandong Academy of Medical Sciences, Jinan 250062, P. R. China. E-mail: mengfinder@mail.ipc.ac.cn
[d] School of Chemistry and Chemical Engineering, Beijing Institute of Technology, Beijing 100081, P. R. China. E-mail: xiaoyanzheng@bit.edu.cn

† Electronic supplementary information (ESI) available: Materials and methods; ^{1}H NMR, ^{13}C NMR, and HRMS spectra; crystallographic data; and photophysical data and imaging data. CCDC 2220486, 2246282, and 2246283. For ESI and crystallographic data in CIF or other electronic format see DOI: https://doi.org/10.1039/d2tc05266k

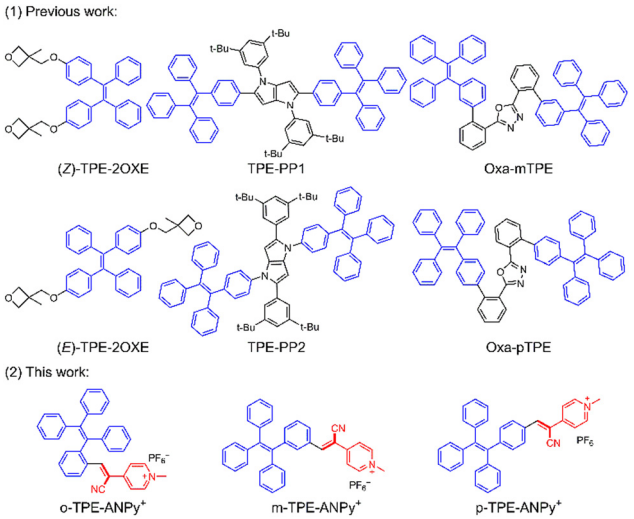

Scheme 1 Structures of TPE-based AIE-active regioisomers reported in previous work and this work.

Wu *et al.* synthesized two oxetane-substituted TPE regioisomers, (*Z*)-TPE-2OXE and (*E*)-TPE-2OXE.[46] Optical and imaging data revealed that (*Z*)-TPE-2OXE exhibited more red-shifted and brighter solid-state emissions than (*E*)-TPE-2OXE. Gryko and co-workers developed two fluorescent regioisomeric AIEgens (TPE-PP1 and TPE-PP2) by conjugating TPE with pyrrolo[3,2-*b*]pyrrole moieties.[45] They found that the different conjugations of TPE greatly influenced the emission properties by entirely different changes in dihedral angles upon excitation, in turn affecting the radiative rate constants, allowed transitions, and HOMO/LUMO distribution.

To the best of our knowledge, scarce attention has been focused on the conjugation or modification of TPE at its *ortho*/*meta*/*para* positions to construct fluorescent regioisomers for their photophysical and application investigations.[47–49] For instance, Li and co-workers developed two regioisomeric AIEgens (Oxa-*m*TPE and Oxa-*p*TPE) by linking basic TPE units to the oxadiazole core through the meta and para positions.[49] The regioisomerism distinctly affected the intramolecular conjugation of Oxa-*p*TPE and Oxa-*m*TPE, which was reflexed by their deep-blue and blue solid-state emissions, respectively. Further use of these AIE regioisomers for non-doped OLEDs with good efficiencies was investigated. Considering the importance of fundamental research and potential applications, there still exists considerable room to explore novel TPE-based AIE regioisomers. Recently, acrylonitriles have emerged as a new building block to develop donor–acceptor-based AIEgens, because of their facile synthesis and easy purification.[50–53] We anticipated that conjugation of TPE at *ortho*/*meta*/*para* positions with the basic acrylonitrile skeleton could lead to new AIE-active regioisomers, which has not been explored so far.

Herein, we synthesized three cationic fluorescent regioisomers (*o*-TPE-ANPy$^+$, *m*-TPE-ANPy$^+$, and *p*-TPE-ANPy$^+$) with an *ortho*-/*meta*-/*para*-substituted electron-withdrawing group (pyridinium-conjugated acrylonitrile) on the phenyl unit of tetraphenylethylene. The regioisomeric effect on the photophysical characteristics and the solid-state intermolecular interactions of these AIEgens was systematically investigated using absorption and fluorescence spectroscopy, DFT calculations, and crystal structures. We applied *o*-TPE-ANPy$^+$ as an example for achieving distinct mechanochromic performance with fluorescence changing from yellow to orange. Moreover, these positively charged AIEgens served as biocompatible probes for wash-free and light-up imaging mitochondria in live cells.

Results and discussion

Synthesis and characterization

The regioisomeric AIEgens were successfully synthesized according to the synthetic route shown in Fig. 1A. First, compound **1** was reacted with different aldehyde group-substituted phenylborates by a Suzuki coupling reaction to give the intermediates **3a**, **3b**, and **3c**. Then these intermediates were reacted with 4-pyridine acetonitrile in the presence of *t*-BuOK in the anhydrous ethanol solution *via* Knoevenagel condensation to form the compounds **5a**, **5b**, and **5c**. Subsequent methylation and anion substitution of the compounds **5a**, **5b**, and **5c** were performed to obtain the final *o*-TPE-ANPy$^+$, *m*-TPE-ANPy$^+$, and *p*-TPE-ANPy$^+$, respectively. The structures of all intermediates and final products were confirmed by ^{1}H NMR, ^{13}C NMR, and HRMS (Fig. S1–S21, ESI†). In addition, their structures were also confirmed by single-crystal structure analysis (Fig. 1B). The details of the X-ray experimental conditions, cell data, and refinement data are summarized in Table S1–S3 (ESI†).

Photophysical properties

We first measured the absorption and fluorescence of these tetraphenylethylene-based acrylonitriles in the THF solution and solid state (Fig. 2 and Table 1). From *o*-TPE-ANPy$^+$ and *m*-TPE-ANPy$^+$ to *p*-TPE-ANPy$^+$, the maximum absorption peak (λ_{abs}) gradually red-shifted (Fig. 2A). The λ_{abs} of *o*-TPE-ANPy$^+$, *m*-TPE-ANPy$^+$, and *p*-TPE-ANPy$^+$ was 320 nm, 348 nm, and 425 nm, respectively. These data indicated that the strong intramolecular charge transfer (ICT) process of *p*-TPE-ANPy$^+$ leads to a lower energy gap. Given the many free rotors of these acrylonitriles, they showed faint emissions in THF (Fig. 2B–D). The fluorescence quantum yield (QY) of *o*-TPE-ANPy$^+$, *m*-TPE-ANPy$^+$, and *p*-TPE-ANPy$^+$ was calculated to be 0.9%, 0.4%, and 0.4%, respectively. We also measured the fluorescence lifetime and estimated their radiative and nonradiative decay rate (Table 1) according to a previous study.[54] Compared with *o*-TPE-ANPy$^+$ and *p*-TPE-ANPy$^+$, *m*-TPE-ANPy$^+$ exhibited a relatively short lifetime and strong nonradiative decay rate, which indicated that the molecules of *m*-TPE-ANPy$^+$ tended to move freely in the solution. In contrast to the faint emissions in solution, the fluorescence of these compounds in the solid state was remarkably boosted, due to the restriction of intramolecular motion (RIM). *o*-TPE-ANPy$^+$ and *m*-TPE-ANPy$^+$ emitted yellow emissions with maximum emission peaks (λ_{em}) of 538 nm and 505 nm, respectively. However, *p*-TPE-ANPy$^+$ with a lower energy gap showed red emissive solid-state fluorescence (λ_{em} of 616 nm). Remarkably, these acrylonitriles, especially *o*-TPE-ANPy$^+$ and

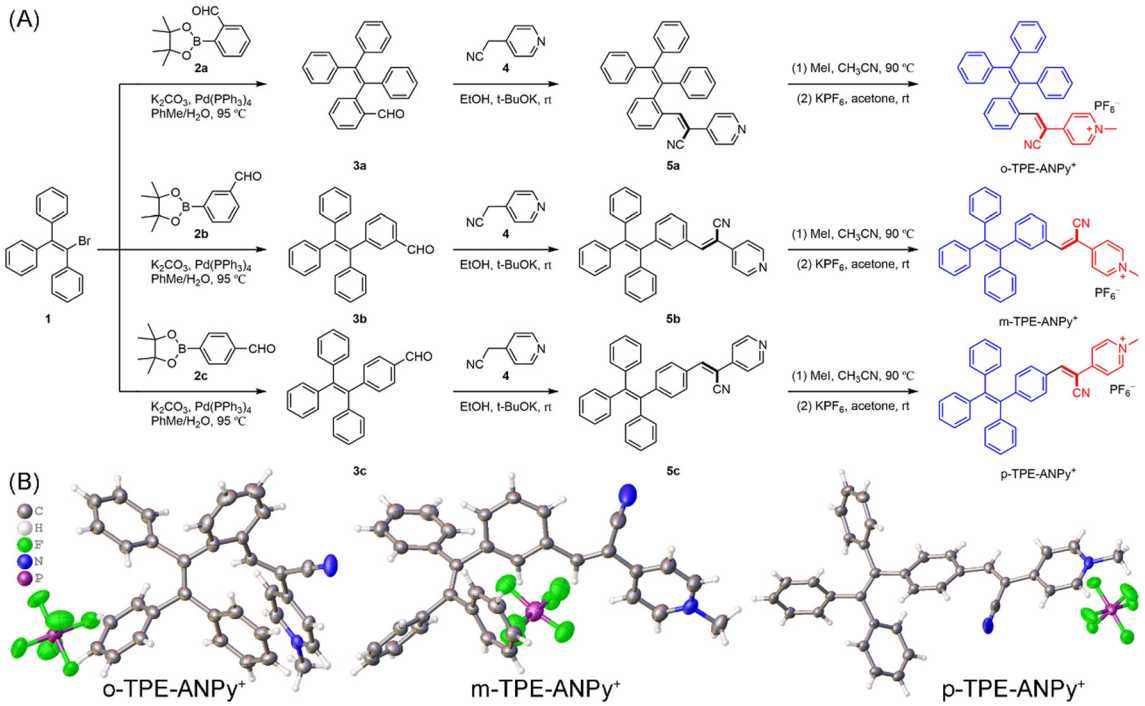

Fig. 1 (A) Synthetic routes to *o*-TPE-ANPy$^+$, *m*-TPE-ANPy$^+$, and *p*-TPE-ANPy$^+$ and (B) their single-crystal X-ray structures. C, gray; H, white; F, green; N, blue; and P, purple.

p-TPE-ANPy$^+$, exhibited high fluorescence QYs of up to 17.2% in the solid state. Interestingly, *m*-TPE-ANPy$^+$ showed a low fluorescence QY of 1.8%, indicating that the meta position of TPE modified by acrylonitrile caused loose packing and strong intramolecular motions. Compared with the faint emissions in the THF solution, the boosted solid-state emissions of *o*-TPE-ANPy$^+$, *m*-TPE-ANPy$^+$, and *p*-TPE-ANPy$^+$ indicate these acrylonitriles are AIE-active.

In addition, the AIE properties of *o*-TPE-ANPy$^+$, *m*-TPE-ANPy$^+$, and *p*-TPE-ANPy$^+$ were further verified in THF/Et_2O mixtures with different Et_2O fractions (f_e) (Fig. 3). Taking *o*-TPE-ANPy$^+$ as an example, it showed weak emission in pure THF, due to free molecular motions; with the increased f_e in THF, its fluorescence intensity barely increased (Fig. 3A and D). When f_e exceeded 90%, the fluorescence at 526 nm of *o*-TPE-ANPy$^+$ increased distinctly, and its λ_{em} reached a maximum at f_e = 99%. Such dramatic fluorescence enhancement was due to the formation of aggregates, in which the free molecular motions were restricted to allow the radiation channel open. The formed aggregates were confirmed by dynamic light scattering (DLS) data (Fig. 3E). Similarly, *m*-TPE-ANPy$^+$ and *p*-TPE-ANPy$^+$ also showed boosted emissions in the THF/Et_2O mixture with a high f_e of 99% (Fig. 3B–D), which were confirmed by DLS data (Fig. S22, ESI†).

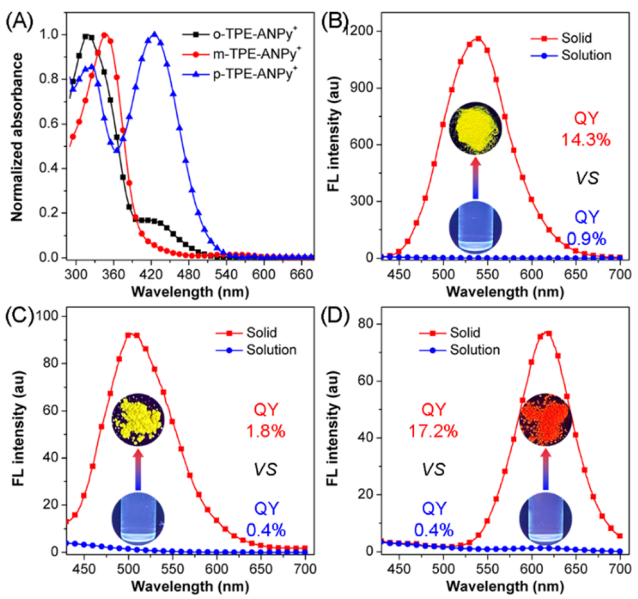

Fig. 2 (A) Normalized absorption spectra of *o*-TPE-ANPy$^+$, *m*-TPE-ANPy$^+$, and *p*-TPE-ANPy$^+$ in THF. Fluorescence spectra of (B) *o*-TPE-ANPy$^+$, (C) *m*-TPE-ANPy$^+$, and (D) *p*-TPE-ANPy$^+$ in the solution and solid state. The insets in (B–D) show solution-state and solid-state fluorescent photos of *o*-TPE-ANPy$^+$, *m*-TPE-ANPy$^+$, and *p*-TPE-ANPy$^+$, respectively, taken under 365 nm UV irradiation. Concentration: 10 μM.

Table 1 Photophysical properties of *o*-TPE-ANPy$^+$, *m*-TPE-ANPy$^+$, and *p*-TPE-ANPy$^+$ in THF

Compound	λ_{abs} (nm)	λ_{em} (nm)	Φ^b (%)	τ^c (ns)	$k_r{}^d$ (10^6 s^{-1})	$k_{nr}{}^e$ (10^8 s^{-1})
o-TPE-ANPy$^+$	320	ND^a	0.9	4.21	2.14	2.35
m-TPE-ANPy$^+$	348	~430	0.4	4.14	0.97	2.41
p-TPE-ANPy$^+$	425	612	0.4	4.21	0.95	2.37

^{a} ND = Not detected. ^{b} Φ is the fluorescence quantum yield. ^{c} τ is the fluorescence lifetime. ^{d} Radiative decay rate $k_r = \Phi/\tau$. ^{e} Nonradiative decay rate $k_{nr} = (1 - \Phi)/\tau$.

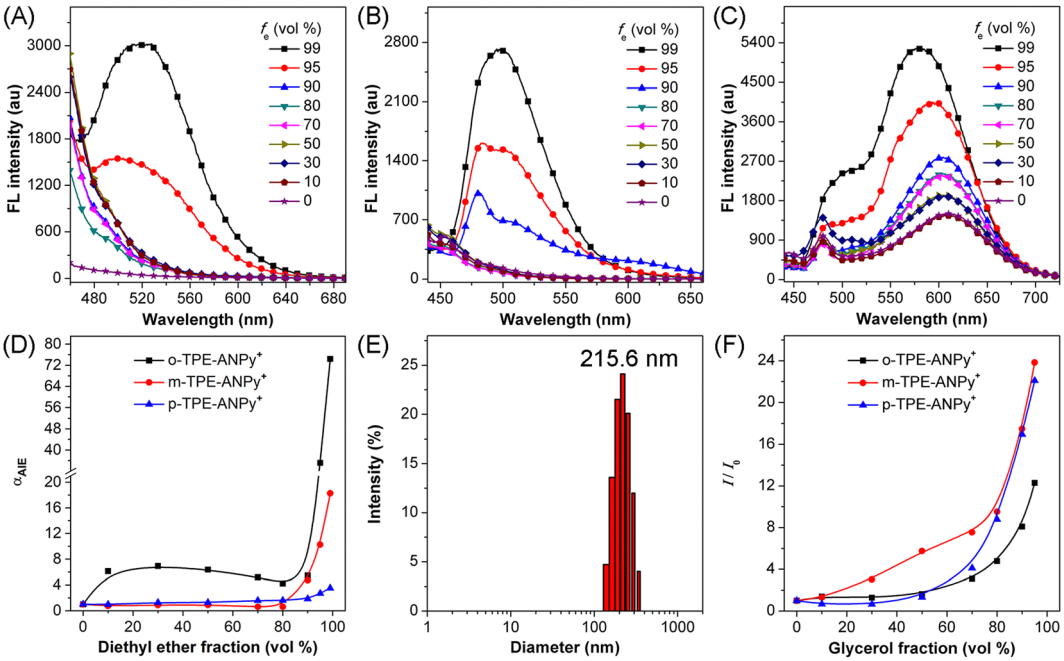

Fig. 3 Fluorescence spectra of (A) *o*-TPE-ANPy$^+$, (B) *m*-TPE-ANPy$^+$, and (C) *p*-TPE-ANPy$^+$ in the THF/Et_2O mixture with different Et_2O fractions (f_e). (D) Plots of α_{AIE} (fluorescence intensity I/I_0) *versus* the composition of the THF/Et_2O mixtures of AIEgens. (E) DLS analysis of *o*-TPE-ANPy$^+$ in the THF/Et_2O mixture containing 99% Et_2O. (F) Relative fluorescence intensity (I/I_0) *versus* the composition of the water/glycerol mixtures (containing 0.25% DMSO) with different glycerol fractions. Concentration: 10 μM.

It should be noted that their fluorescence at high f_e was slightly blue-shifted compared with that in pure THF, due to the solvatochromic effect of these ICT-based dyes.[55,56] These data confirmed that these regioisomeric acrylonitriles belong to the AIEgen family.

According to the RIM mechanism, AIEgens with free rotor motions in the solution state should be sensitive to viscosity changes.[17] To test this, we studied the fluorescence of *o*-TPE-ANPy$^+$, *m*-TPE-ANPy$^+$, and *p*-TPE-ANPy$^+$ in water/glycerol mixtures with different glycerol fractions (f_g) to exhibit different viscosities. As shown in Fig. S23 (ESI†) and Fig. 3F, these AIEgens exhibited negligibly weak fluorescence in the aqueous solution. With the increased f_g in water, the viscosity of water/glycerol mixtures was increased, and the fluorescence intensities of our AIEgens gradually increased accordingly. As expected, a significant increase in fluorescence intensities was observed for these AIEgens at a high f_g of 95%, and *m*-TPE-ANPy$^+$ and *p*-TPE-ANPy$^+$ showed comparable fluorescence enhancements (23.8 and 22.1 fold for *m*-TPE-ANPy$^+$ and *p*-TPE-ANPy$^+$, respectively), more significant than *o*-TPE-ANPy$^+$ (12.3 fold) (Fig. 3F). Interestingly, the fluorescence of AIEgens was slowly increased when f_g was below 70%, while their fluorescence significantly increased after f_g = 70%, indicating that these AIEgens are more sensitive to high-viscosity environments. These results suggested that the regioisomeric acrylonitriles are sensitive to viscosity changes and can serve as excellent fluorescent probes to light up viscous environments in live samples in a wash-free manner.

To better investigate the optical properties of these AIEgens, we conducted density generalized function theory (DFT) calculations. The DFT calculations were performed at the theoretical level of ωB97XD/6-31G (d,p) using the Gaussian 09 program package. As shown in Fig. 4A, the HOMO orbitals of *o*-TPE-ANPy$^+$ and *m*-TPE-ANPy$^+$ are distributed on the TPE part at the optimized ground states, while those of *p*-TPE-ANPy$^+$ are delocalized on the whole molecule, resulting in a greater HOMO energy level of *p*-TPE-ANPy$^+$. On the other hand, the LUMO orbitals of these AIEgens are mainly distributed on the acrylonitrile unit, indicating apparent ICT effects. Their calculated DFT data at the optimized ground states are summarized in Table S4 (ESI†). *o*-TPE-ANPy$^+$ and *m*-TPE-ANPy$^+$ exhibited a strongly allowed $S_0 \rightarrow S_2$ absorption transition with an oscillator strength (f) of 0.3068 and 0.9126, respectively. However, an allowed $S_0 \rightarrow S_1$ absorption transition (f = 0.9527) was dominant for *p*-TPE-ANPy$^+$. The calculated absorption variation tendencies were in good agreement with the photophysical data (Table 1). In addition, the geometries of these AIEgens at the ground states and excited states were optimized by time-dependent (TD)-DFT at the ωB97XD/6-31G (d,p) level (Fig. 4B). The root mean square displacement (RMSD) was estimated to evaluate the molecular dynamics. The calculated RMSD data of *m*-TPE-ANPy$^+$ were larger than those of *o*-TPE-ANPy$^+$ and *p*-TPE-ANPy$^+$. The reorganization energy between the ground and excited states is also summarized in Table S5 (ESI†). *m*-TPE-ANPy$^+$ had a larger reorganization energy than other AIEgens. Taken together, the significantly large RMSD and reorganization energy data demonstrated the strong intramolecular motions of *m*-TPE-ANPy$^+$, leading to the strongest nonradiative decay rate and the worst emission behaviour among these regioisomers.

We also analyzed the intermolecular interaction and packing of *o*-TPE-ANPy$^+$, *m*-TPE-ANPy$^+$, and *p*-TPE-ANPy$^+$ in the crystal

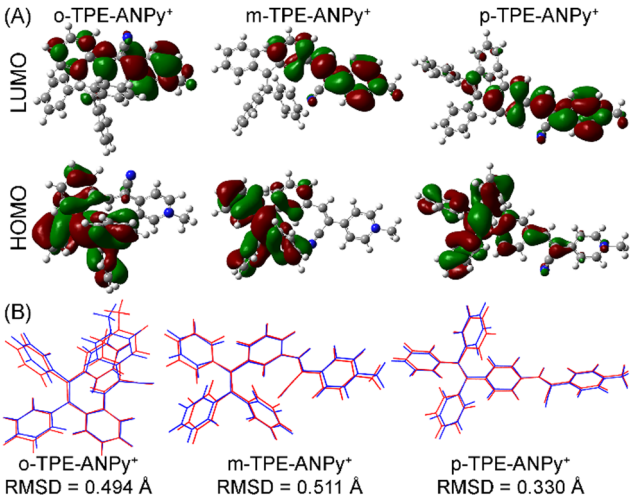

Fig. 4 (A) Spatial electron distributions of HOMOs and LUMOs of our AIEgens at the optimized ground states at the ωB97XD/6-31G (d,p) level. (B) The structural superposition and RMSD values of our AIEgens in the ground states (blue color) and excited (red color) geometries.

state to explain its strong solid-state emission (Fig. 5). These AIEgens adopted staggered parallel packing in the crystal lattice. However, no face-to-face π–π interactions were observed, because of the highly twisted molecular structure and long intermolecular distance. For *p*-TPE-ANPy$^+$, only weak π–π interactions existed between two adjacent staggered molecules. Multiple intermolecular interactions, including C–H···F, C–H···N, C–H···π, C–Cl···π, P–F···π, and unusual C≡N···π interactions, contributed to the RIM and rigid structures, further leading to boosted solid-state fluorescence. Compared with *o*-TPE-ANPy$^+$ and *p*-TPE-ANPy$^+$, the intermolecular interactions to restrict the molecular motions of TPE parts of *m*-TPE-ANPy$^+$ were less, which was probably the reason for the low solid-state fluorescence.

Mechanochromism

Considering the highly twisted structures of TPE derivatives, it is speculated that these AIE regioisomers may have mechanochromic behavior.[17] We first pre-checked their emission changes on filter paper rubbed with hands. Interestingly, *o*-TPE-ANPy$^+$ exhibited notable emission changes under external pressure stimuli, while the fluorescence of other isomers barely changed. Encouraged by this preliminary data, we carefully studied their mechanochromic behaviors mechanically ground with an agate mortar. After strong grinding of *o*-TPE-ANPy$^+$, distinct emission color changes from yellow to orange were observed under the irradiation of a UV lamp (Fig. 6A). In contrast, compared with *o*-TPE-ANPy$^+$, both *m*-TPE-ANPy$^+$ and *p*-TPE-ANPy$^+$ displayed slight variations in emissions after grinding (Fig. S24, ESI†), which may be due to their less twisted structures and less possibility of transformation from a twisted to planar structure under external pressure. The λ_{em} of the ground powder of *o*-TPE-ANPy$^+$ was determined to be 582 nm, a red shift of 53 nm compared to the yellow-emissive pristine solid sample with λ_{em} of 529 nm (Fig. 6B), indicating satisfying mechanochromic performance. The fluorescence QY of the ground samples of *o*-TPE-ANPy$^+$ was decreased to 3.24%, because of the formed loose packing and enhanced non-radiation rate. After fumigation with dichloromethane vapor, the original samples of *o*-TPE-ANPy$^+$can be restored from the corresponding ground samples (Fig. 6 and Fig. S25, ESI†), revealing its reversible mechanochromic behavior. Given the highly twisted structures and multiple weak intermolecular interactions that exist in the crystal structures (Fig. 5), we anticipated that strong grinding could destroy these weak interactions and make *o*-TPE-ANPy$^+$ prone to transform from the crystalline to the microcrystal or amorphous state under external stimuli, further leading to the good π–conjugation structure and distinct red-shifted color changes.[57] Compared with original samples, the ground samples of *o*-TPE-ANPy$^+$ showed red-shifted absorption (Fig. S26, ESI†), further confirming better π–conjugation structures after grinding. To better understand the mechanochromic performance of *o*-TPE-ANPy$^+$, powder X-ray diffraction (XRD) experiments were performed before and after grinding. As shown in Fig. 6C, the XRD pattern of the *o*-TPE-ANPy$^+$ pristine solid sample showed intense sharp diffraction peaks. After strong grinding, however, most diffraction peaks almost disappeared and the intensity of the remaining diffraction peaks was greatly decreased. These data confirmed that strong grinding disrupts the highly ordered crystalline structure of *o*-TPE-ANPy$^+$ and leads to the structural transition to microcrystals, further resulting in distinct emission color changes.

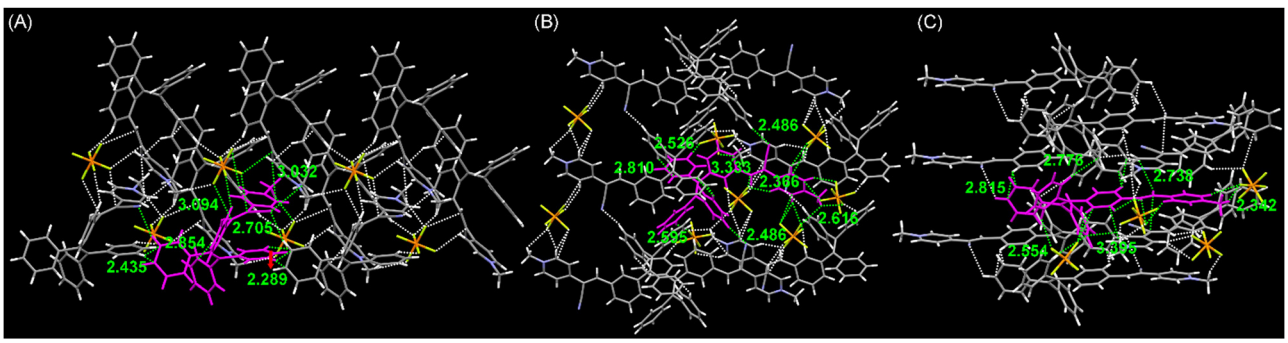

Fig. 5 Intermolecular packing and interactions in the crystal of (A) *o*-TPE-ANPy$^+$, (B) *m*-TPE-ANPy$^+$, and (C) *p*-TPE-ANPy$^+$. The molecules of interest shown in purple color. The intermolecular interactions between the molecule of interest and others shown in green dashed lines. Distances in Å.

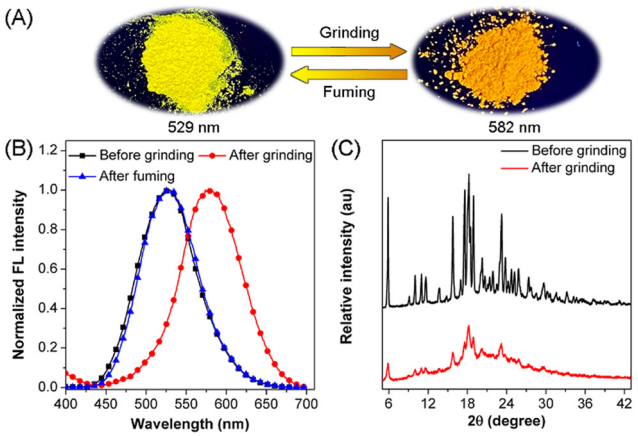

Fig. 6 (A) Solid-state fluorescent photos of *o*-TPE-ANPy$^+$ upon grinding and fuming (dichloromethane vapor). (B) Fluorescence spectra and (C) XRD patterns of *o*-TPE-ANPy$^+$ under different conditions. Fluorescent photos were taken under 365 nm UV irradiation.

Wash-free bioimaging

Inspired by the strong fluorescence of these AIEgens in the aggregated state and restricted environments, we further investigated their potential use for biological applications. The cytotoxicity of the AIEgens on HeLa cells was first determined by the standard MTT method. After incubation for 24 h, the MTT data showed that the survival rate of HeLa cells remained above 87% even at high concentrations up to 10 μM (Fig. S27, ESI†), indicating their low cytotoxicity and good biocompatibility. Then, the *in vitro* live cell imaging experiments were conducted using a confocal laser scanning microscope (CLSM). After incubation in HeLa cells for 2 h without washing, it was found that all three AIEgens could fluoresce intracellularly and the fluorescence was likely from the mitochondria (Fig. S28, ESI†). Almost no emission signals were observed outside the cell, revealing their wash-free and light-up imaging capabilities. Increasing results have indicated that positively charged dyes generally stain the mitochondria by electrostatic interactions.[58–60] To confirm the speculation, we co-incubated each of our AIEgens with a commercial mitochondrial probe MitoTracker Deep Red. The co-localization results showed that the emission channels of AIEgens well overlapped with MitoTracker Deep Red, with a Pearson correlation coefficient of 0.88, 0.86, and 0.93 for *o*-TPE-ANPy$^+$, *m*-TPE-ANPy$^+$, or *p*-TPE-ANPy$^+$, respectively (Fig. 7). Apparently, these AIEgens can specifically stain mitochondria in live cells.

Conclusions

In summary, three cationic tetraphenylethylene-based regioisomeric acrylonitriles (*o*-TPE-ANPy$^+$, *m*-TPE-ANPy$^+$, and *p*-TPE-ANPy$^+$) featuring AIE properties were facilely synthesized. The regioisomeric effect on the photophysical properties and the solid-state intermolecular interactions of these acrylonitriles was systematically investigated using absorption and fluorescence spectroscopy, DFT calculations, and crystal structures. They emitted faint emissions in solution, while the fluorescence in the solid state was boosted with a QY of up to 17.2%. Interestingly, *m*-TPE-ANPy$^+$ exhibited low emissions in the solution and solid state, indicating that the meta position of the TPE modified by acrylonitrile causes strong intramolecular motion. Due to the different ICT effects, *p*-TPE-ANPy$^+$ showed more red-shifted

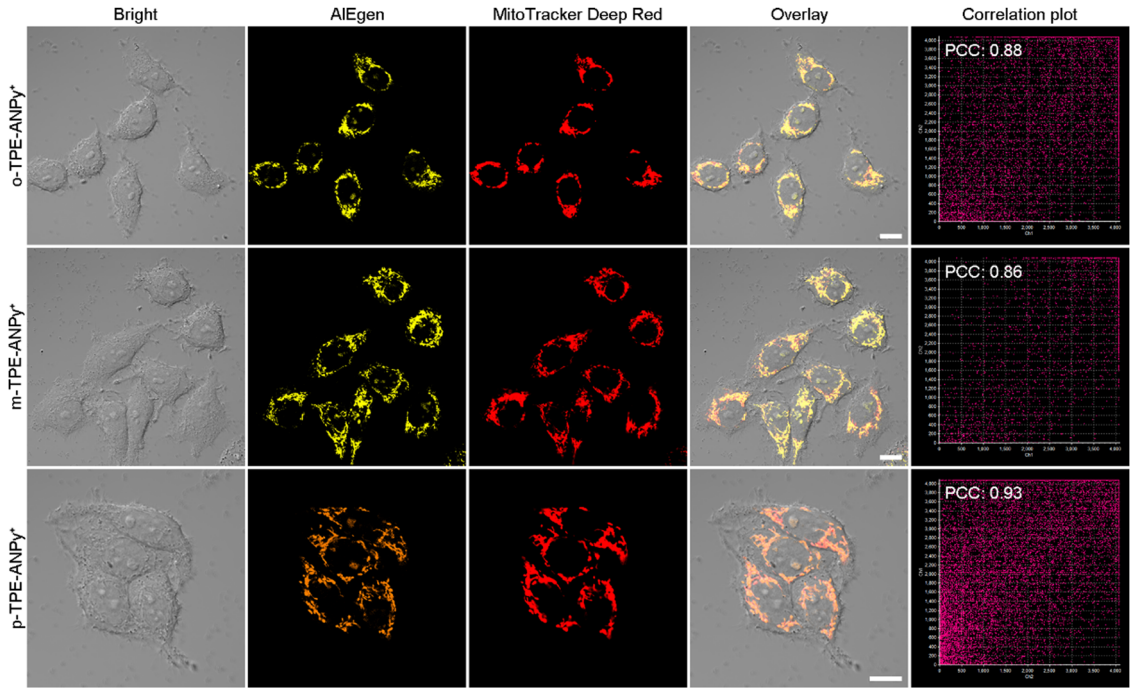

Fig. 7 CLSM images of HeLa cells incubated with *o*-TPE-ANPy$^+$, *m*-TPE-ANPy$^+$, or *p*-TPE-ANPy$^+$ (8 μM) and MitoTracker Deep Red (100 nM). PCC: Pearson's correlation coefficient. Scale bar: 10 μm.

emission than the other regioisomeric acrylonitriles in both solution and solid states. In addition, the fluorescence enhancements of *m*-TPE-ANPy$^+$ and *p*-TPE-ANPy$^+$ are more significant toward viscosity than *o*-TPE-ANPy$^+$. Moreover, *o*-TPE-ANPy$^+$ was applied for achieving reversible mechanochromic performance with fluorescence changing from yellow to orange. Further use of these biocompatible AIEgens for wash-free and light-up imaging of mitochondria wase successfully demonstrated. This work provides new insights into developing fluorescent regioisomeric materials with tunable photophysical properties for diverse applications in optoelectronic and biological fields.

Conflicts of interest

There are no conflicts to declare.

Acknowledgements

This work was supported by the National Natural Science Foundation of China (62105184), the Natural Science Foundation of Jiangsu Province, China (BK20210107), the Natural Science Foundation of Shandong Province, China (2022HWYQ-007, ZR2021QB043, and ZR2022QB149), and the Special Fund of Taishan Scholars Project of Shandong Province, China (tsqn201909012). We thank Prof. Xiaobo Huang from Wenzhou University for helping measure the solid-state UV-vis absorption spectra and giving valuable suggestions in the mechanochromism part. We also thank Prof. Xiaoqiang Yu from Shandong University for providing the facilities to conduct confocal imaging experiments.

Notes and references

1 Z. Zhang, M. Kang, H. Tan, N. Song, M. Li, P. Xiao, D. Yan, L. Zhang, D. Wang and B. Z. Tang, *Chem. Soc. Rev.*, 2022, **51**, 1983–2030.
2 J. Zhang, B. He, Y. Hu, P. Alam, H. Zhang, J. W. Y. Lam and B. Z. Tang, *Adv. Mater.*, 2021, **33**, 2008071.
3 J. Ochi, K. Tanaka and Y. Chujo, *Angew. Chem., Int. Ed.*, 2020, **59**, 9841–9855.
4 S.-J. Zou, Y. Shen, F.-M. Xie, J.-D. Chen, Y.-Q. Li and J.-X. Tang, *Mater. Chem. Front.*, 2020, **4**, 788–820.
5 B. He, B. Situ, Z. Zhao and L. Zheng, *Small Methods*, 2020, **4**, 1900583.
6 X. Huang, L. Qian, Y. Zhou, M. Liu, Y. Cheng and H. Wu, *J. Mater. Chem. C*, 2018, **6**, 5075–5096.
7 J. Zhao, Z. Chi, Y. Zhang, Z. Mao, Z. Yang, E. Ubba and Z. Chi, *J. Mater. Chem. C*, 2018, **6**, 6327–6353.
8 C. Wang and Z. Li, *Mater. Chem. Front.*, 2017, **1**, 2174–2194.
9 X. Zhao, Q. Yao, S. Long, W. Chi, Y. Yang, D. Tan, X. Liu, H. Huang, W. Sun, J. Du, J. Fan and X. Peng, *J. Am. Chem. Soc.*, 2021, **143**, 12345–12354.
10 K.-X. Teng, W.-K. Chen, L.-Y. Niu, W.-H. Fang, G. Cui and Q.-Z. Yang, *Angew. Chem., Int. Ed.*, 2021, **60**, 19912–19920.
11 L. Xing, B. Wang, J. Li, X. Guo, X. Lu, X. Chen, H. Sun, Z. Sun, X. Luo, S. Qi, X. Qian and Y. Yang, *J. Am. Chem. Soc.*, 2022, **144**, 2114–2119.
12 J. L. Belmonte-Vázquez, Y. A. Amador-Sánchez, L. A. Rodríguez-Cortés and B. Rodríguez-Molina, *Chem. Mater.*, 2021, **33**, 7160–7184.
13 M. K. Bera, P. Pal and S. Malik, *J. Mater. Chem. C*, 2020, **8**, 788–802.
14 J. Luo, Z. Xie, J. W. Y. Lam, L. Cheng, H. Chen, C. Qiu, H. S. Kwok, X. Zhan, Y. Liu, D. Zhu and B. Z. Tang, *Chem. Commun.*, 2001, 1740–1741.
15 G. Jiang, J. Yu, J. Wang and B. Z. Tang, *Aggregate*, 2022, **3**, e285.
16 G. Niu, R. Zhang, X. Shi, H. Park, S. Xie, R. T. K. Kwok, J. W. Y. Lam and B. Z. Tang, *TrAC, Trends Anal. Chem.*, 2020, **123**, 115769.
17 J. Mei, N. L. C. Leung, R. T. K. Kwok, J. W. Y. Lam and B. Z. Tang, *Chem. Rev.*, 2015, **115**, 11718–11940.
18 B.-K. An, J. Gierschner and S. Y. Park, *Acc. Chem. Res.*, 2012, **45**, 544–554.
19 G. Feng and B. Liu, *Acc. Chem. Res.*, 2018, **51**, 1404–1414.
20 X. Nie, W. Huang, D. Zhou, T. Wang, X. Wang, B. Chen, X. Zhang and G. Zhang, *Aggregate*, 2022, **3**, e165.
21 S. Ito, M. Gon, K. Tanaka and Y. Chujo, *Natl. Sci. Rev.*, 2021, **8**, nwab049.
22 J. Qi, H. Ou, Q. Liu and D. Ding, *Aggregate*, 2021, **2**, 95–113.
23 Y. Sun and P. J. Stang, *Aggregate*, 2021, **2**, e94.
24 Z. Guo, C. Yan and W.-H. Zhu, *Angew. Chem., Int. Ed.*, 2020, **59**, 9812–9825.
25 Q. Li and Z. Li, *Acc. Chem. Res.*, 2020, **53**, 962–973.
26 M. Chen, A. Qin, J. W. Y. Lam and B. Z. Tang, *Coord. Chem. Rev.*, 2020, **422**, 213472.
27 H.-T. Mao, G.-F. Li, G.-G. Shan, X.-L. Wang and Z.-M. Su, *Coord. Chem. Rev.*, 2020, **413**, 213283.
28 M. Martínez-Abadía, R. Giménez and M. B. Ros, *Adv. Mater.*, 2018, **30**, 1704161.
29 H.-T. Feng, Y.-X. Yuan, J.-B. Xiong, Y.-S. Zheng and B. Z. Tang, *Chem. Soc. Rev.*, 2018, **47**, 7452–7476.
30 D. D. La, S. V. Bhosale, L. A. Jones and S. V. Bhosale, *ACS Appl. Mater. Interfaces*, 2018, **10**, 12189–12216.
31 Z. Yang, Z. Chi, Z. Mao, Y. Zhang, S. Liu, J. Zhao, M. P. Aldred and Z. Chi, *Mater. Chem. Front.*, 2018, **2**, 861–890.
32 L. Xu, X. Long, J. He, L. Liu, F. Kang, Z. Deng, J. Wu, X.-F. Jiang, J. Wang and Q. Zhang, *J. Mater. Chem. C*, 2023, DOI: **10.1039/D2TC03928A**.
33 L. Xu, X. Long, F. Kang, Z. Deng, J. He, S. Yang, J. Wu, L. Yin, X.-F. Jiang, F. Lu, M.-D. Li and Q. Zhang, *J. Mater. Chem. C*, 2022, **10**, 7039–7048.
34 B. Roy, I. Maisuls, J. Zhang, F. C. Niemeyer, F. Rizzo, C. Wölper, C. G. Daniliuc, B. Z. Tang, C. A. Strassert and J. Voskuhl, *Angew. Chem., Int. Ed.*, 2022, **61**, e202111805.
35 X. Long, J. Wu, S. Yang, Z. Deng, Y. Zheng, W. Zhang, X.-F. Jiang, F. Lu, M.-D. Li and L. Xu, *J. Mater. Chem. C*, 2021, **9**, 11679–11689.
36 P. Yao, Y. Wang, W. Qiao, X. Sun, H. Peng, X. Xie and Z. A. Li, *J. Mater. Chem. C*, 2021, **9**, 13687–13696.
37 C. Li, M. Hanif, X. Li, S. Zhang, Z. Xie, L. Liu, B. Yang, S. Su and Y. Ma, *J. Mater. Chem. C*, 2016, **4**, 7478–7484.

38 K. Wu, T. Zhang, L. Zhan, C. Zhong, S. Gong, Z.-H. Lu and C. Yang, *Adv. Opt. Mater.*, 2016, **4**, 1558–1566.
39 X. Zhang, Z. Ma, X. Li, C. Qian, Y. Liu, S. Wang, X. Jia and Z. Ma, *ACS Appl. Mater. Interfaces*, 2021, **13**, 40986–40994.
40 H.-X. Yu, J. Zhi and J.-L. Wang, *J. Mater. Chem. C*, 2021, **9**, 3882–3891.
41 Z. Guo, J. Zhao, Y. Liu, G. Li, H. Wang, Y. Hou, M. Zhang, X. Li and X. Yan, *Chin. Chem. Lett.*, 2021, **32**, 1691–1695.
42 H. Wei, Y. Yu, Y. Wang, Z. Ying, W. Cheng, X. Tian and Q. Kan, *Sens. Actuators, B*, 2020, **321**, 128536.
43 M. Li, F. Peng, L. Ying and J. Xu, *J. Mater. Chem. C*, 2019, **7**, 3553–3559.
44 X. Hu, H. Chen, L. Zhao, M. Miao and Y. Zheng, *Chem. Mater.*, 2019, **31**, 10256–10262.
45 B. Sadowski, K. Hassanein, B. Ventura and D. T. Gryko, *Org. Lett.*, 2018, **20**, 3183–3186.
46 X. Fang, Y.-M. Zhang, K. Chang, Z. Liu, X. Su, H. Chen, S. X.-A. Zhang, Y. Liu and C. Wu, *Chem. Mater.*, 2016, **28**, 6628–6636.
47 L. Wen, C. Zang, Y. Gao, Y. Tao, G. Li, G. Shan, H. Sun, W. Xie and Z. Su, *Dyes Pigm.*, 2020, **173**, 107912.
48 J. Yang, J. Huang, Q. Li and Z. Li, *J. Mater. Chem. C*, 2016, **4**, 2663–2684.
49 J. Huang, P. Chen, X. Yang, R. Tang, L. Wang, J. Qin and Z. Li, *Sci. China: Chem.*, 2013, **56**, 1213–1220.
50 S. Cao, X. Tian, M. Cao, J. Wang, G. Niu and B. Z. Tang, *Chem. Mater.*, 2023, **35**, 2472–2485.
51 M. Liu, Y. Chen, Y. Guo, H. Yuan, T. Cui, S. Yao, S. Jin, H. Fan, C. Wang, R. Xie, W. He and Z. Guo, *Nat. Commun.*, 2022, **13**, 2179.
52 G. Niu, X. Zheng, Z. Zhao, H. Zhang, J. Wang, X. He, Y. Chen, X. Shi, C. Ma, R. T. K. Kwok, J. W. Y. Lam, H. H. Y. Sung, I. D. Williams, K. S. Wong, P. Wang and B. Z. Tang, *J. Am. Chem. Soc.*, 2019, **141**, 15111–15120.
53 C. Y. Y. Yu, H. Xu, S. Ji, R. T. K. Kwok, J. W. Y. Lam, X. Li, S. Krishnan, D. Ding and B. Z. Tang, *Adv. Mater.*, 2017, **29**, 1606167.
54 W.-Q. Zheng, K.-Y. Lu, X.-Q. Gan, H. Zhang, X.-Q. Yan, J.-T. Yu, Y.-F. Wang, X.-G. Wu and W.-G. Zhu, *J. Mater. Chem. C*, 2023, **11**, 4017–4024.
55 C.-J. Wu, X.-Y. Li, T. Zhu, M. Zhao, Z. Song, S. Li, G.-G. Shan and G. Niu, *Anal. Chem.*, 2022, **94**, 3881–3887.
56 M. Cao, T. Zhu, M. Zhao, F. Meng, Z. Liu, J. Wang, G. Niu and X. Yu, *Anal. Chem.*, 2022, **94**, 10676–10684.
57 Y. Chen, C. Dai, X. Xu, Y. Zhou, Y. Lei, M. Liu, W. Gao, X. Huang and H. Wu, *J. Phys. Chem. C*, 2021, **125**, 24180–24188.
58 C. Chen, R. Zhang, J. Zhang, Y. Zhang, H. Zhang, Z. Wang, X. Huang, S. Chen, R. T. K. Kwok, J. W. Y. Lam, D. Ding and B. Z. Tang, *CCS Chem.*, 2022, **4**, 2249–2257.
59 Q. Li, J. Gong, Y. Li, R. Zhang, H. Wang, J. Zhang, H. Yan, J. W. Y. Lam, H. H. Y. Sung, I. D. Williams, R. T. K. Kwok, M.-H. Li, J. Wang and B. Z. Tang, *Chem. Sci.*, 2021, **12**, 709–717.
60 Z. He, Y. Gao, H. Zhang, Y. Xue, F. Meng and L. Luo, *Adv. Healthcare Mater.*, 2021, **10**, 2101056.